DNS OF SINGLE BUBBLE MOTION IN LIQUID METAL AND THE INFLUENCE OF A MAGNETIC FIELD

Stephan Schwarz
Institute of Fluid Mechanics
TU Dresden
01062 Dresden, Germany
Stephan.Schwarz@tu-dresden.de

Jochen Fröhlich
Institute of Fluid Mechanics
TU Dresden
01062 Dresden, Germany
Jochen.Froehlich@tu-dresden.de

ABSTRACT

The ascent of a single Argon bubble in a column of quiescent liquid metal is studied by means of direct numerical simulation using an immersed boundary method. An additional magnetic field in the direction of gravity is shown to influence the bubble dynamics substantially. An increase in time-averaged bubble Reynolds number is found for large bubbles and a decrease for small bubbles when increasing the magnetic interaction parameter. The bubble Strouhal number as a dimensionless frequency is reduced with magnetic field for all bubbles considered. The zig-zag trajectory in the purely hydrodynamic case becomes more rectilinear and vortical structures in the bubble wake are considerably damped.

INTRODUCTION

The combination of multiphase and magneto-hydrodynamic (MHD) flows povides a complex and challenging field of large interest. Liquid metals, however, are opaque so that experimental data are difficult to obtain. Simulations are hence essential to support the measurements and provide further insight and understanding.

There is a variety of industrial MHD applications where gas bubbles play an important role, for instance metallurgical processes. Within the continuous casting process, gas bubbles are injected into the melt to clean the liquid metal from contaminants and to stirr and homogenize the liquid phase. Magnetic fields are used for this process to stirr and to stabilize the flow regimes. The actual influence of the magnetic field on the bubbles is still not fully understood.

A single bubble can be characterized by the Galilei number $G = \sqrt{g\,d_{eq}^3}/\nu$ and Eötvös number $Eo = \Delta\rho\, g\, d_{eq}^2/\sigma$. The resulting bubble rise velocity u_p can then be used to determine the bubble Reynolds number $Re = u_p\, d_{eq}/\nu$ and Weber number $We = \rho_f\, {u_p}^2\, d_{eq}/\sigma$, where g is gravity, d_{eq} the diameter of a volume-equivalent sphere, ν kinematic viscosity of the liquid, $\Delta\rho$ density difference between the phases, ρ_f density of the surrounding fluid and σ surface tension. For gas bubbles in liquid metals high $Re \approx 3000-5000$ and $We \approx 3$ are encountered resulting in an ellipsoidal whobbling shape according to the regime map of Clift *et al.* (1978). The strength of a magnetic field can be characterized by the magnetic interaction parameter $N = \sigma_e B^2 d_{eq}/\left(\rho_f u_{ref}\right)$ with σ_e being the electrical conductivity, B the magnetic field strength and $u_{ref} = \sqrt{g\,d_{eg}}$ the reference velocity for a rising bubble.

COMPUTATIONAL METHOD

Simulations were conducted with the multiphase code PRIME (Kempe & Fröhlich, 2010*a*,*b*) which is based on a staggered grid arrangement in cartesian coordinates employing a second order finite volume method. The incompressible Navier-Stokes equations including the Lorentz force

$$\nabla \cdot \mathbf{u} = 0 \tag{1}$$

$$\frac{\partial \mathbf{u}}{\partial t} + (\mathbf{u}\cdot\nabla)\,\mathbf{u} = -\frac{1}{\rho_f}\nabla p + \frac{1}{Re}\nabla^2\mathbf{u} + N\,(\mathbf{j}\times\mathbf{B}) + \mathbf{f} \tag{2}$$

are solved using a Runge-Kutta three-step method with implicit treatment of the viscous terms. The Lorentz force is determined solving a second Poisson equation for the magnetic potential under the low magnetic Reynolds number assumption.

Bubbles are represented by an Euler-Lagrangian approach, specifically the immersed boundary method (IBM) of Uhlmann (2005) with extension to non-spherical particles and low particle densities (Kempe *et al.*, 2009). The motion of

each single bubble is determined solving its linear and angular momentum equation

$$m_p \frac{d\mathbf{u}_p}{dt} = \rho_f \oint_\Gamma \boldsymbol{\tau}\cdot\mathbf{n}\, ds + V_p(\rho_p - \rho_f)\,\mathbf{g} \qquad (3)$$

$$\frac{d\left(\mathbf{I}_p\boldsymbol{\omega}_p\right)}{dt} = \rho_f \oint_\Gamma \mathbf{r}\times(\boldsymbol{\tau}\cdot\mathbf{n})\, ds\,. \qquad (4)$$

The surface integrals in (3), (4) are obtained from the momentum equation of the underlying fluid and the resulting volume integrals are determined efficiently using the signed-distance level set function of the particle surface for the cut cell volumes (Kempe *et al.*, 2009). To describe the motion of a non-spherical (e.g. ellipsoidal) object, one has to account for its inertial tensor, whereas for a sphere the moments of inertia are solely described by a single scalar. The inertial tensor needs to be transformed according to the orientation of the particle $\mathbf{I}_p = f(\phi_i, t)$ in each step of the time integration scheme when solving in the laboratory coordinate system.
Coupling between the phases is realized by means of surface markers, so that arbitrary shapes can be considered. Here, positioning of forcing points is performed by surface triangulation with a commercial grid generator. At the bubble surface a no-slip boundary condition is applied, motivated by the fact that in liquid metals an oxyde layer occurs at the interface between gas and liquid.
In the present work, the bubble shape is approximated as an oblate ellipsoid of aspect ratio $X = a/b$ with semi-axes $a = c > b$ (Figure 1).
During the ascent, the shape of the ellipsoidal particle is modified in time according to a correlation for its aspect ratio X based on the instantaneous bubble Weber number. To this end, the data in Loth (2008) were fitted by

$$X^{-1}(t) = 1 - 0.75\tanh(0.155582\,We(t)). \qquad (5)$$

With this approach the bubble volume is conserved exactly. The method allows to directly model the bubble shape. This is a useful feature since bubble shapes in contaminated systems (as gas - liquid metal) are not fully understood to date.

In this study, the electrical conductivity for both phases is modelled to be the same for technical reasons. This is adequate as the focus lies on the influence of a magnetic field on the bubble wake.

GRID STUDY

The influence of the discretization has been studied in a cubical box of extend $L = 6.0\,d_{eq}$ with n^3 gridpoints. The initial acceleration of a single bubble with a Galilei number of $G = 2825$ and an Eötvös number of $Eo = 2.5$ is considered which is examined in more detail in a larger computational domain below. The reference grid has a resolution of $n = 512$, this corresponds to $d_{eq}/\Delta x = 85.3$ gridpoints over the equivalent diameter of the bubble. The timestep is refined as well based on a constant CFL number as well.

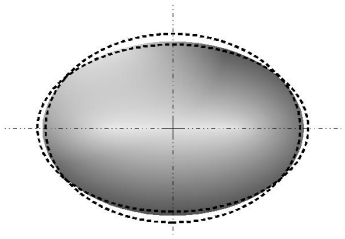

Figure 1. Ellipsoidal bubble undergoing a shape oscillation. The dotted lines indicate the states with maximum and minimum aspect ratio observed in the simulation with $N = 0$ reported below.

To quantify the discretization error, the particle Reynolds number is compared at $t' = 1.0$ with the value on the finest grid chosen as reference. The grid chosen for the simulations in the large box of $n = 256$ yields an error of about 3% compared to the finest grid. A convergence order of about 1.7 has been determined based on the fit in Figure 3. The timescale of the acceleration of the particle is longer on a coarser grid. A coarse resolution leads to higher terminal Reynolds numbers (see Figure 2).

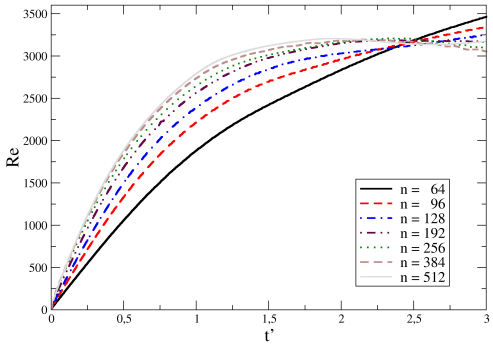

Figure 2. Bubble Reynolds number over time as a function of grid spacing, $N = 0$.

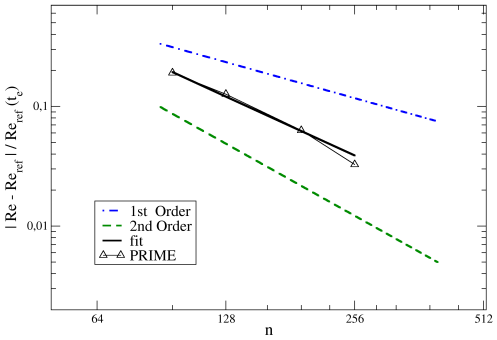

Figure 3. Relative error in Re at $t' = 1.0$, for the simulation in Figure 2.

RESULTS

In Zhang *et al.* (2005) an experiment was conducted releasing a single argon bubble at the bottom of a container filled with liquid metal (GaInSn), and its position during the rise was measured by ultrasound Doppler velocimetry. The physical parameters of that experiment are $G = 2825$, $Eo = 2.5$ obtained with $d_{eq} = 4.6$ mm. Measurements were conducted without a magnetic field as well as with a field oriented in vertical direction, i.e. parallel to gravity. This was found to influence the bubble dynamics.

Single bubble without magnetic field

The simulation was performed in a box of $\mathbf{L} = (6.0, 30.0, 6.0)\,d_{eq}$ with periodic boundary conditions in all three directions. The spatial resolution is $\mathbf{n} = (256, 1280, 256)$, i.e. 83.9 Mio grid points, $n_L = 9093$ Lagrangian forcing points were positioned on the bubble surface, the time step is $\Delta t' = 2.5 \cdot 10^{-3}$ in dimensionless units using $t_{ref} = \sqrt{d_{eq}/g}$. With the present method, only a moderate runtime of 60×61.5 CPU hours on an SGI Altix 4700 is required for one crossing of the above box requiring about 30 dimensionless units in time.

After an initial acceleration the bubble rise velocity starts to oscillate (Figure 4). The time-averaged Reynolds number after the initial transient is called the terminal Reynolds number Re_t. A quantitative comparison with the experiment of Zhang

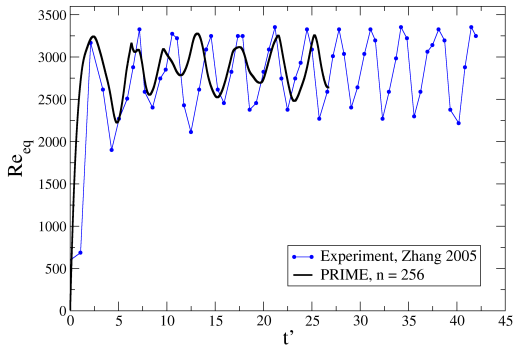

Figure 4. Bubble Reynolds number over time and comparison to experimental data of Zhang *et al.* (2005) for $N = 0$, $t' = t/t_{ref}$

et al. (2005) is given in Table 1. Excellent agreement is obtained for the time-averaged value of Re, i.e. the terminal rise velocity. An underprediction of the amplitude of the oscillation is observed, measured by the standard deviation σ_{Re}. Good agreement on the other hand is found in the dominant frequency of the oscillation f'_{Re}. A zig-zag trajectory with lateral drift (Figure 5) and an oscillation in bubble inclination (Figure 6) were found. These data could not be measured in the experiment. The amplitude of the zig-zag of ca. $1.15\,d_{eq}$ and the maximum inclination angle $|\phi_z|_{max} \approx 36°$ of the bubble agree well with data from the literature for other gas-liquid systems. From the literature, the lateral distance between two extreme points in a zig-zag trajectory is reported as approxi-

Table 1. Results for single bubble without magnetic field compared to experimental data of Zhang *et al.* (2005). $\langle Re \rangle$ is the temporally averaged Reynolds number, σ_{Re} the corresponding standard deviation and $f_{ref} = \sqrt{g/d_{eq}}$.

	Re_t	σ_{Re}	$f'_{Re} = f/f_{ref}$
Simulation	2871	245	0.276
Zhang *et al.* (2005)	2879	369	0.280

mately $1.0 - 1.3\,d_{eq}$ and the maximum inclination to be about $27 - 30°$ (Gaudlitz & Adams, 2007; Lunde & Perkins, 1998; Brücker, 1999; Mougin & Magnaudet, 2006). The inclination angle in the present simulation is slightly higher, possibly due to the higher Reynolds number.

After the initial transient the aspect ratio of the ellipsoid oscillates in the interval $X \in (1.35,\ 1.57)$ as shown in Figure 1.

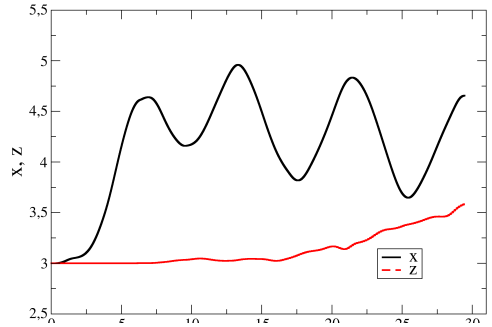

Figure 5. Zig-zag trajectory for $N = 0$. History of lateral bubble center coordinates x and z, non-dimensionalized with d_{eq}.

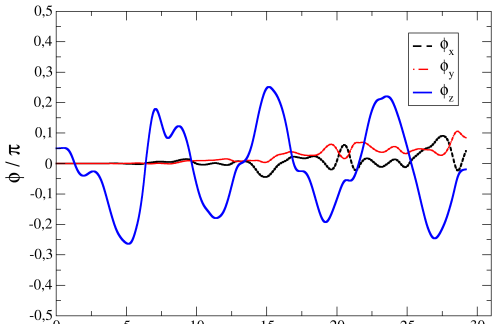

Figure 6. Bubble orientation over time described by the angles of orientation for $N = 0$.

A smaller bubble was studied in a second series of numerical experiments. The physical parameters are $G = 1488$, $Eo = 1.05$ which corresponds to a $d_{eq} = 3.0$ mm Argon bubble in GaInSn. The shape of the latter bubble remains almost spherical due to the dominant role

of surface tension. A time-averaged Reynolds number of $Re_t = 1822$ was determined from the simulation data. The rise velocity again oscillates and a zig-zag path is oberserved. The charateristic frequency is calculated from a Fourier spectrum of $Re(t)$ being $f' = 0.222$ which is in good agreement with Lindt (1972). No experiments in liquid metal could be conducted for this small bubble for technical reasons.

Single bubble with magnetic field

In further simulations a longitudinal magnetic field in the direction of gravity was applied with $N = 0.5$ and $N = 1.0$. When increasing the magnetic interaction parameter N the bubble motion is affected as follows:

- The time-averaged bubble Reynolds number Re_t increases for large bubbles (high Eo).
- The time-averaged bubble Reynolds number Re_t decreases for small bubbles (low Eo).
- The Strouhal number St decreases for all bubbles.
- The amplitude of oscillation in $Re(t)$ decreases.
- The amplitude of oscillation in lateral coordinates $x(t)$, $z(t)$ decreases, i.e. the trajectory is more rectilinear.
- The amplitude of oscillation in tilting angles $\phi_i(t)$ decreases.
- The plane integral of absolute value of the vertical vorticity component $\langle|\omega_y|\rangle_{xz} = \iint |\omega_y| dx dz$ decreases.

The Strouhal number as a dimensionless frequency is based on the oscillation of $Re(t)$ as in the experiments.
All these findings are in agreement with conclusions from the experiments by Zhang *et al.* (2005). In these experiments, the analysis of vortex structures is difficult, though. In contrast, the present simulations provide full access to all velocity and pressure data for the continuous liquid metal phase as well as precious data concerning the bubble trajectory.
A maximum in $Re(t)$ is reached at the extreme points of the bubble path $x(t)$. The bubble is oriented with its small semi-axis parallel to the gravity vector, i.e. the inclination angle ϕ_z is approximately zero. Maximum tilting of the bubble is achieved closely after a local minimum in $Re(t)$ and approximately half way between the maximum extends of the zig-zag trajectory. At this point, the lateral velocity is largest. The described events are highlighted as dots in Figures 8, 9, 10 and for these instants data are analyzed further.
Substantial damping of the vortical structures in the bubble wake due to the magnetic field is observed. Especially small structures vanish while the larger vortex filaments are aligned with the magnetic field. A qualitative assessment of the vortical structures is given in Figure 7. The iso-contours correspond to positive and negative values of the vorticity component in direction of gravity. The snapshots are taken at extreme points of the zig-zag trajectory.

A quantification of the damping effect in the bubble wake is provided in Figure 11. The absolute value of the vorticity component ω_y is integrated in xz-planes and plotted over the vertical distance from the bubble center. The instants in time correspond to similar points in the bubble trajectory indicated as dots in Figures 8 - 10. It can be seen that with increasing magnetic interaction the bubble wake contains less vertical vorticity and the values of the extrema in the plot are

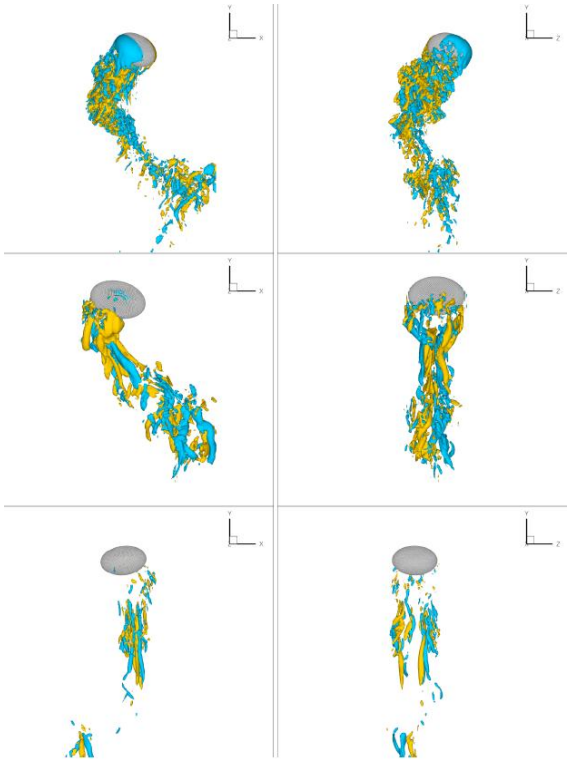

Figure 7. Instantaneous iso-contures of the vertical vorticity component ω_y as a function of the magnitude of the magnetic field, $N = 0,\ 0.5,\ 1.0$ (top to bottom), $G = 2825$, $Eo = 2.5$. Left and right picture provide complementary views of the same structure at two angles differing by 90°.

substantially reduced. Figures 12 and 13 provide analogous data for the other two vorticity components. The plots show global maximum values of $\langle|\omega_x|\rangle_{xz}$ and $\langle|\omega_z|\rangle_{xz}$ at the front of the bubble in all cases and considerable damping of vorticity in the wake in the presence of a magnetic field. A comparison with experimental data by Zhang *et al.* (2005) is given in Figure 14 and 15. Here, the simulations labelled with 'coarse' have been conducted using an isotropic grid of step size 1.5 times the one of the companion grid, i.e. $n_x = 192$.
The results are in good agreement showing an increase in terminal Reynolds number for large bubbles and a decrease in Re_t for small bubbles with increasing magnetic interaction parameter. This is due to the adverse effects of the magnetic field increasing the drag of an object as shown by Maxworthy (1968), but supressing lateral dynamics in the trajectory. Also the absolute changes in Re_t agree well with the observations in the experiments. Nevertheless, the measurements reveal a different threshold Eo for the reversion of the trend (Re_t increases or decreases with N) at slightly larger Eötvös numbers.
A decrease of the bubble Strouhal number St is found for all bubble sizes and interaction parameters. In the simulation, the relative change in St is less pronounced for small bubbles than for large bubbles. An overprediction of the reduction in St in the simulation is recognized at large magnetic interaction parameters.

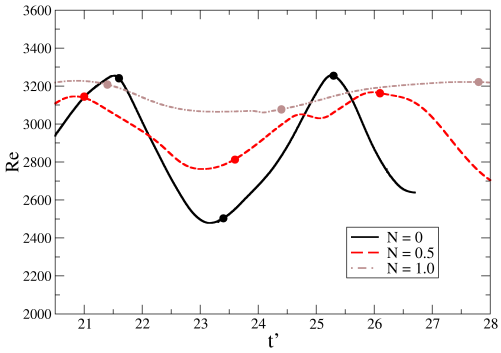

Figure 8. History of bubble Reynolds number for the three cases $N = 0,\ 0.5,\ 1.0$ and $G = 2825$, $Eo = 2.5$.

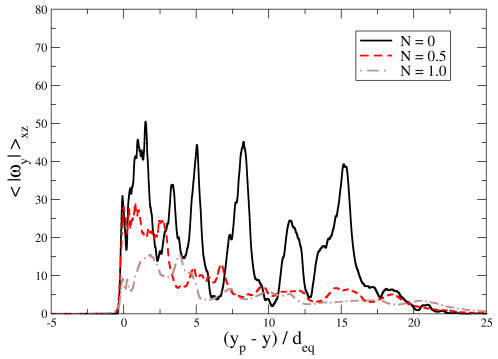

Figure 11. Plane integral of absolute vertical vorticity component $\langle|\omega_y|\rangle_{xz}$ for the third event indicated in Figures 8 - 10, for the three cases $N = 0,\ 0.5,\ 1.0$ with $G = 2825$, $Eo = 2.5$.

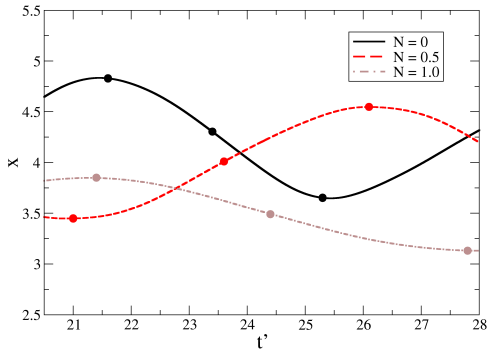

Figure 9. Zig-zag trajectory, history of lateral bubble center coordinates x non-dimensionalized with d_{eq}, for the three cases $N = 0,\ 0.5,\ 1.0$ and $G = 2825$, $Eo = 2.5$.

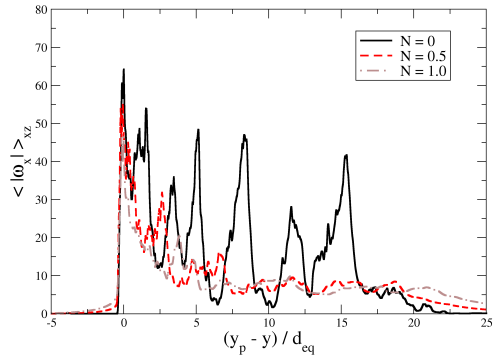

Figure 12. As Figure 11 but for $\langle|\omega_x|\rangle_{xz}$.

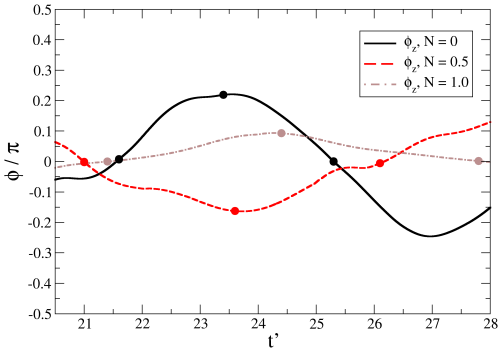

Figure 10. History of inclination angle ϕ_z, for the three cases $N = 0,\ 0.5,\ 1.0$ and $G = 2825$, $Eo = 2.5$.

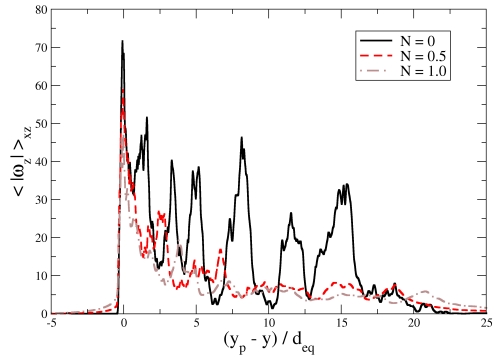

Figure 13. As Figure 11 but for $\langle|\omega_z|\rangle_{xz}$.

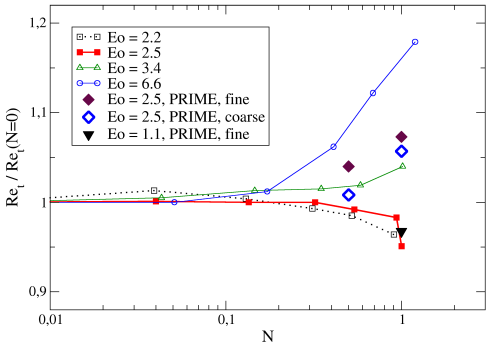

Figure 14. Relative change in terminal Reynolds number: Present simulations compared to experimental data by Zhang *et al.* (2005).

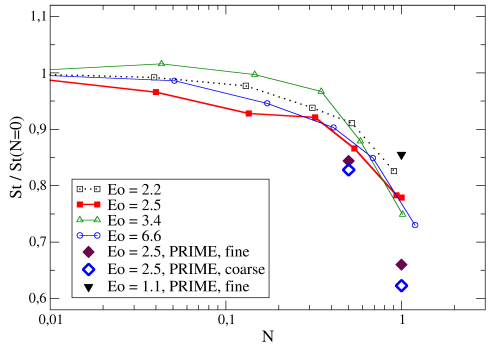

Figure 15. Relative change in Strouhal number: Present simulations compared to experimental data by Zhang *et al.* (2005).

CONCLUSIONS AND OUTLOOK

The ascent of a single bubble in liquid metal has been successfully simulated. All observations from the corresponding experiments of Zhang *et al.* (2005) were retrieved and could be elucidated by additional data from the simulations. A detailed view has been given on the vortical structures in the wake of the bubble under the influence of a longitudinal magnetic field.

Further simulations will be conducted with variable bubble shape based on spherical harmonic functions allowing more complex bubble forms. With this approach, the bubble shape is calculated directly from the fluid loads of the surrounding liquid metal enabling the simulation of bubble chains and swarms in liquid metal.

ACKNOWLEDGEMENTS

The present work is funded by DFG through the collaborative research center SFB 609. Computing time was provided by ZIH, Dresden. The authors thank S. Eckert for providing his experimental data in electronic form and helpful discussions on the experiments.

REFERENCES

Brücker, C. 1999 Structure and dynamics of the wake of bubbles and its relevance for bubble interaction. *Phys. Fluids* **11**.

Clift, R., Grace, J.R. & Weber, M.E. 1978 *Bubbles, Drops, and Particles*. Dover Publications.

Gaudlitz, Daniel & Adams, Nikolaus A. 2007 Two-phase flow computations by the hybrid particle-level-set method. *5th Int. Symp. Turbulence and Shear Flow Phenomena* **Vol. 1**.

Kempe, T. & Fröhlich, J. 2010*a* On euler-lagrange coupling and collision modelling for spherical particles. *8th Int. ERCOFTAC Symp. on Engineering Turbulence Modelling and Measurements, Marseille, France* .

Kempe, T. & Fröhlich, J. 2010*b* Phase-resolved simulation of spherical particles in viscous fluids and their interaction. *12th ERCOFTAC Workshop on two-phase flow predictions, Halle-Wittenberg, Germany* .

Kempe, T., Schwarz, S. & Fröhlich, J. 2009 Modelling of spheroidal particles in viscous flow. *Academy Colloquium Immersed Boundary Methods: Current Status and Future Research Directions. Amsterdam, the Netherlands* .

Lindt, J. T. 1972 On the periodic nature of the drag on a rising bubble. *Chem. Eng. Sci.* **27** (10), 1775 – 1781.

Loth, E. 2008 Quasi-steady shape and drag of deformable bubbles and drops. *Int. J. Multiphase Flow* **34**, 523–546.

Lunde, Knud & Perkins, Richard 1998 Shape oscillations of rising bubbles. *Appl. Sci. Res.* **58**, 387–408.

Maxworthy, T. 1968 Experimental studies in magneto-fluid dynamics: Pressure distribution measurements around a sphere. *J. Fluid Mech.* **31**, 801–814.

Mougin, Guillaume & Magnaudet, Jacques 2006 Wake-induced forces and torques on a zigzagging/spiralling bubble. *J. Fluid Mech.* **567**, 185–194.

Uhlmann, M. 2005 An immersed boundary method with direct forcing for the simulation of particulate flows. *J. of Comp. Phys.* **209**.

Zhang, C., Eckert, S. & Gerbeth, G. 2005 Experimental study of single bubble motion in a liquid metal column exposed to a dc magnetic field. *Int. J. Multiphase Flow* **106**.